Data Article

Data on ultrabright fluorescent cellulose acetate nanoparticles for imaging tumors through systemic and topical applications

Berney Peng [a,1,2], Mohammad Almeqdadi [b,c,d,2],
Fabrice Laroche [e], Shajesh Palantavida [f,3], Maxim Dokukin [f,4],
Jatin Roper [c,d], Omer H. Yilmaz [c], Hui Feng [e], Igor Sokolov [a,f,g,*]

[a] Department of Biomedical Engineering, Tufts University, Medford, MA, USA
[b] Department of Medicine, St. Elizabeth's Medical Center, Boston, MA, USA
[c] The David H. Koch Institute for Integrative Cancer Research at MIT, Cambridge, MA, USA
[d] Department of Medicine, Tufts Medical Center, Boston, MA, USA
[e] Departments of Pharmacology and Medicine, The Center for Cancer Research, Section of Hematology and Medical Oncology, Boston University School of Medicine, Boston, MA, USA
[f] Department of Mechanical Engineering, Tufts University, Medford, MA, USA
[g] Department of Physics, Tufts University, Medford, MA, USA

ARTICLE INFO

ABSTRACT

Characterization data of fluorescent nanoparticles made of cellulose acetate (CA-dots) are shown. The data in this article accompanies the research article "*Ultrabright fluorescent cellulose acetate nanoparticles for imaging tumors through systemic and topical applications*" [1]. The measurements and calculation of brightness of individual CA-dots are presented. The description of conjugation procedure Pluronic F127-Folic Acid copolymer and folic acid is shown. Identification of composition of CA dots using Raman and absorbance spectroscopy is demonstrated. The methods for image analysis of efficiency of CA-dot targeting of epithelial tumors xenografted in zebrafish is presented.

Specifications table

Subject area	*Materials Science*
More specific subject area	*Cellulose acetate fluorescent nanoparticles*
Type of data	*Tables, images*
How data was acquired	*Absorbance and fluorescent spectrometers (Horiba, Agilent), Raman microscope (Witec), microbalance, particle sizer (Malvern) fluorescent microscope.*
Data format	*Raw, analyzed*
Experimental factors	*Particles were measured dispersed in water (particle characterization included morphology and luminescence); zebrafish were imaged after particles injection (confusion matrix parameters); mice colon were imaged after topical application of particles (observed tumor contrast). Tumor targeting (folate) nanoparticles and material control (PEGylated) nanoparticles were formulated and compared.*
Experimental features	*To collect optical spectra, particle suspension was to avoid self-absorbance and nonlinear response; zebrafish were immobilized in gel for fluorescent imaging. Particle size, surface potential, brightness, and composition were determined. Sensitivity, specificity, and accuracy were calculated from co-registered zebrafish fluorescence images.*
Data source location	*Tufts University, Medford, MA, USA*
Data accessibility	*Data is with this article*
Related research article	*Peng, B., Almeqdadi, M., Laroche, F., Palantavida, S., Dokukin, M., Roper, J., Yilmaz, O. H., Feng, H. & Sokolov, I. Ultrabright fluorescent cellulose acetate nanoparticles for imaging tumors through systemic and topical applications. Materials Today, in press (2018)* [1].

Value of the data

- The scheme illustrated in Fig. 1 can be used to conjugate Pluronic F127 to folic acid and to synthesize functionalized cellulose acetate nanoparticles utilizing the synthesized polymer-FA conjugate.
- The fluorescent brightness calculations can be used to assess the brightness of individual CA-dots.
- The linear combination method of spectra described can be used to identify the composition of CA-dots using a Raman and UV–VIS absorbance spectroscopy.
- The method of image analysis of particle-cancer cell colocalization can be used to calculate the efficiency of nanoparticle targeting, such as sensitivity, specificity, and accuracy.
- The presented data serves as a reference for characterization of physical properties of CA-dots.

1. Data

The data in this article contains the methods of synthesis of guest polymer and polymer-folic acid conjugates used to functionalize CA dots (Fig. 1), examples of Raman (Fig. 2) and absorbance spectra collected on aqueous suspension of CA dots, fluorescent spectra of CA dots (Figs. 3 and 4) and the results of calculation of fluorescent brightness of individual CA dots (Table 1), and the description of the method to define the accuracy of specific targeting of tumors inside zebrafish (Fig. 5) using the folate-functionalized CA dots (Figs. 6, 7, and 8).
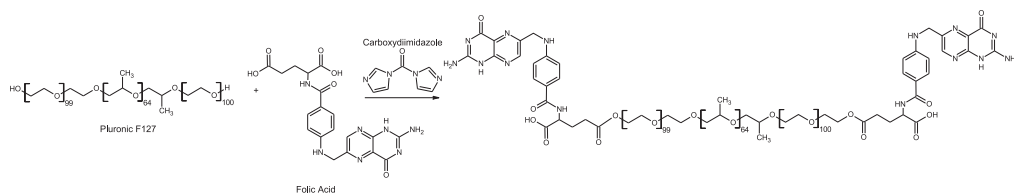
Fig. 1. Conjugation scheme of folic acid and PF127 copolymer.
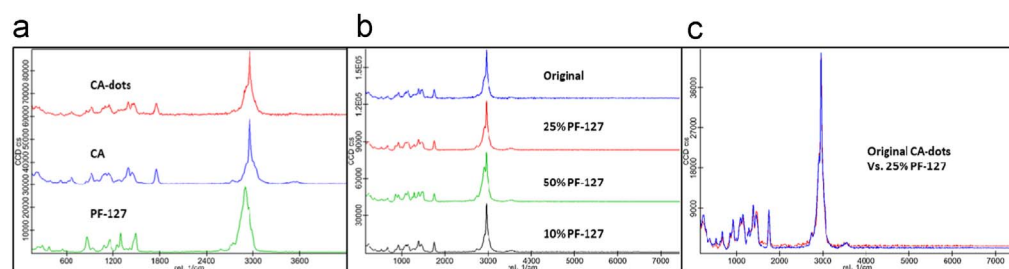
Fig. 2. Raman spectra of individual components and nanoparticles are shown in (a). Raman spectra of nanoparticles of varying compositions (10–50% by weight PF127) were simulated from component spectra and evaluated to fit the original CA-dot spectra in (b). Examples of simulated spectra at 10, 25, and 50% by weight guest polymer are shown. A 25/75% PF-127/CA nanoparticle composition best matched the CA-dot spectra (c).

2. Experimental design, materials, and methods

2.1. Preparation of Pluronic F127-folic acid conjugated polymer

0.20 mmol of Folic acid (FA) in dried DMSO was prepared and added to a one neck flask. Next, Carboxydiimidazole (CDI) was added to make 0.22 mmol concentration, and the reaction mix was stirred for one day at room temperature in the dark. Dehydrated Pluronic F127 (PF-127) was added to the above solution to attain 0.05 mmol concentration. The reaction proceeded in the dark for 1 day at room temperature. The conjugated PF-127-FA polymer solution was dialyzed over 2 days (12 kD Spectrapore membrane in DI water) with dialysate changing every 6 h.

2.2. Measurement of fluorescent brightness of individual CA dots

Particle fluorescence, brightness, and photostability were measured using the FLUOLOG 3 fluorimeter by Horiba and a UV–vis Cary 60 spectrophotometer by Agilent. To characterize fluorescent brightness of nanoparticles, we follow the basic definition of the brightness of fluorophores used in flow cytometry, MESF units (Molecules of Equivalent Soluble Fluorophore). This definition uses the comparison brightness of nanoparticles and a fluorophore of known brightness within the same spectral range (reference fluorophore). Such a definition is independent of a particular spectrometer or methods of measurement. The brightness of a single nanoparticle was calculated using the following formula:

$$\text{Brightness } [MESF\ units] = (FL_{NP}/C_{NP})/(FL_{dye}/C_{dye}), \tag{1}$$

where FL_{NP} or FL_{dye} is the fluorescence intensity of a nanoparticle suspension or reference dye solution, respectively. The spectra of both CA nanoparticles and the reference dye solution are very close (when evaluating brightness, spectra need to be as similar as possible), so the fluorescence units measured from each sample was evaluated by integrating over the same emission wavelength interval, see Refs. [2–4] for more detail.
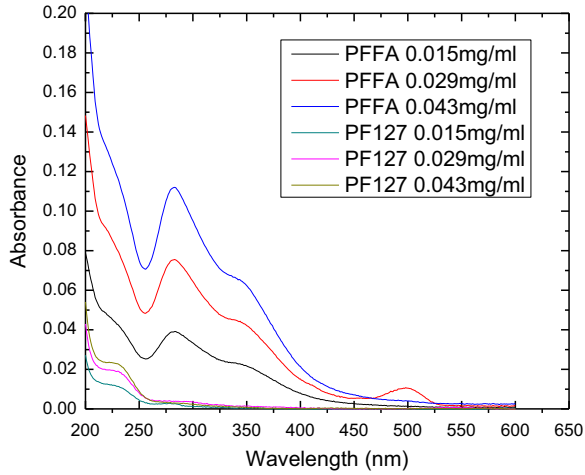
Fig. 3. Absorbance of PF127-folic acid (PFFA) with increase in concentration 0.015 (blue), 0.03 (green) and 0.045 (red) mg/mL and of control PF127 with increase in concentration 0.015 (cyan), 0.03 (purple) and 0.045 (yellow) mg/ml.
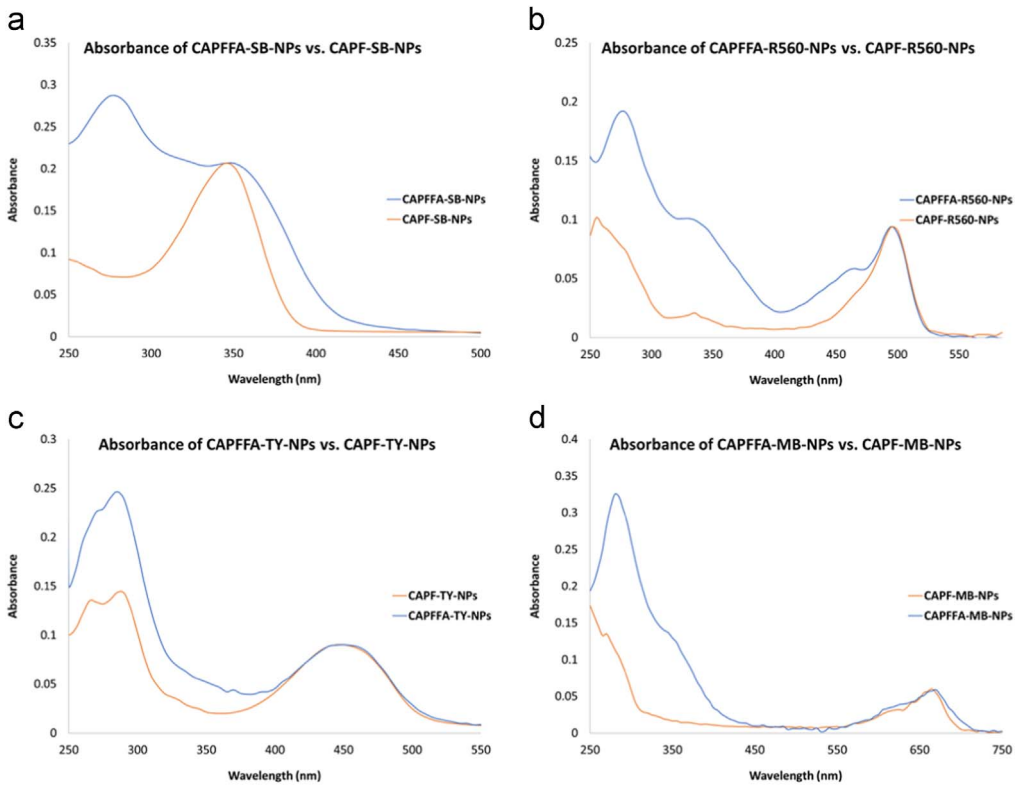
Fig. 4. Absorbance spectra (a) of Stilbene 420, (b) Rhodamine 560, (c) Tracer Yellow, and (d) Methylene Blue encapsulated particles, PEGylated (orange curve) and folate-conjugated (blue curve). All spectra have been normalized to the specific encapsulated dye peak of each particle.

Table 1

Brightness calculations of individual PEGylated and folate-functionalized CA-dots. Fluorescence intensity was measured by integrating across a defined spectrum for both particles and free dye. The relative brightness calculation defines the brightness of a single particle in terms of the effective number of single dye molecules given by Eq. (1).

Particle	Size (nm)	Range of integration of fluorescence (nm)	# Particles Intensity/concentration (CPS)	# Molecules Intensity/concentration (CPS)	Brightness of a single particle (MESF units)
CA-SB-PEG	61	370–600	2.04E + 03	5.15E + 04	90
CA-SB-PEG-FA	50	370–600	1.90E + 02	5.15E + 04	530
CA-GREEN-PEG	77	495–600	2.36E + 04	2.87E + 06	870
CA- GREEN-PEG-FA	68	495–600	1.81E + 04	2.87E + 06	780
CA-YEL-PEG	60	470–650	3.95E + 04	1.87E + 06	160
CA- YEL-PEG-FA	87	470–650	2.96E + 04	1.87E + 06	650
CA-RED/NIR-PEG	77	665–750	1.71E + 05	6.11E + 07	2550
CA- RED/NIR-PEG-FA	63	665–750	7.50E + 05	6.11E + 07	320
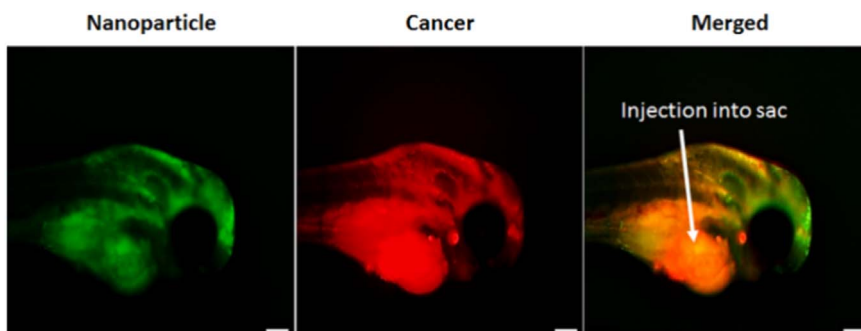
Fig. 5. Fluorescence images of nanoparticle, cancer cell, and merged particle-cancer channels within the zebrafish head. Cervical cancer cells/metastases and targeted nanoparticles were both injected into the sac directly behind the eye. Scale bar is 100 μm.

Stilbene 420 (blue), Rhodamine 560 (green), Tracer Yellow (yellow), Methylene Blue (red/NIR) were used for encapsulation. Data for particles covered with PEG and PEG+folate are shown. The results are shown in Table 1. Each particle name consists of three parts: CA-Color-Coating molecules (CA stands for cellulose acetate). For example, CA-GREEN-PEG means cellulose acetate with encapsulated Rhodamine 560 (green) dye, coated with PEG molecules. CA- GREEN-PEG-FA means the same particle with additionally added folic acid molecules coating such particles.

2.3. Composition of functionalized nanoparticles

A Witec (Ulm, Germany) Alpha 300R series Confocal Raman microscope was used to determine the composition of functionalized nanoparticles with PF-127 polymer. Raman spectra of individual components, cellulose acetate and PF-127, were taken and evaluated against Raman spectra of PEGylated CA-dots. Cellulose acetate and PF-127 samples were measured in native powder form and placed on an aluminum surface while nanoparticle solutions were dried on an aluminum surface. CA-dot spectra were dominated by the presence of the CA core, with contributions of the guest polymer manifesting primarily in the alkyl peak stretches (2700–3000 cm^{-1}).

Simulations utilizing linear combinations of component spectra (CA and PF-127) were performed to minimize residuals and match nanoparticle spectra (see Ref. [5] for detail). It was determined that CA nanoparticles assembled at a 1:1 CA to guest polymer molar ratio, produces a particle concentration of roughly 1–2 mg/mL with a guest polymer composition of 25% by weight (Fig. 2).
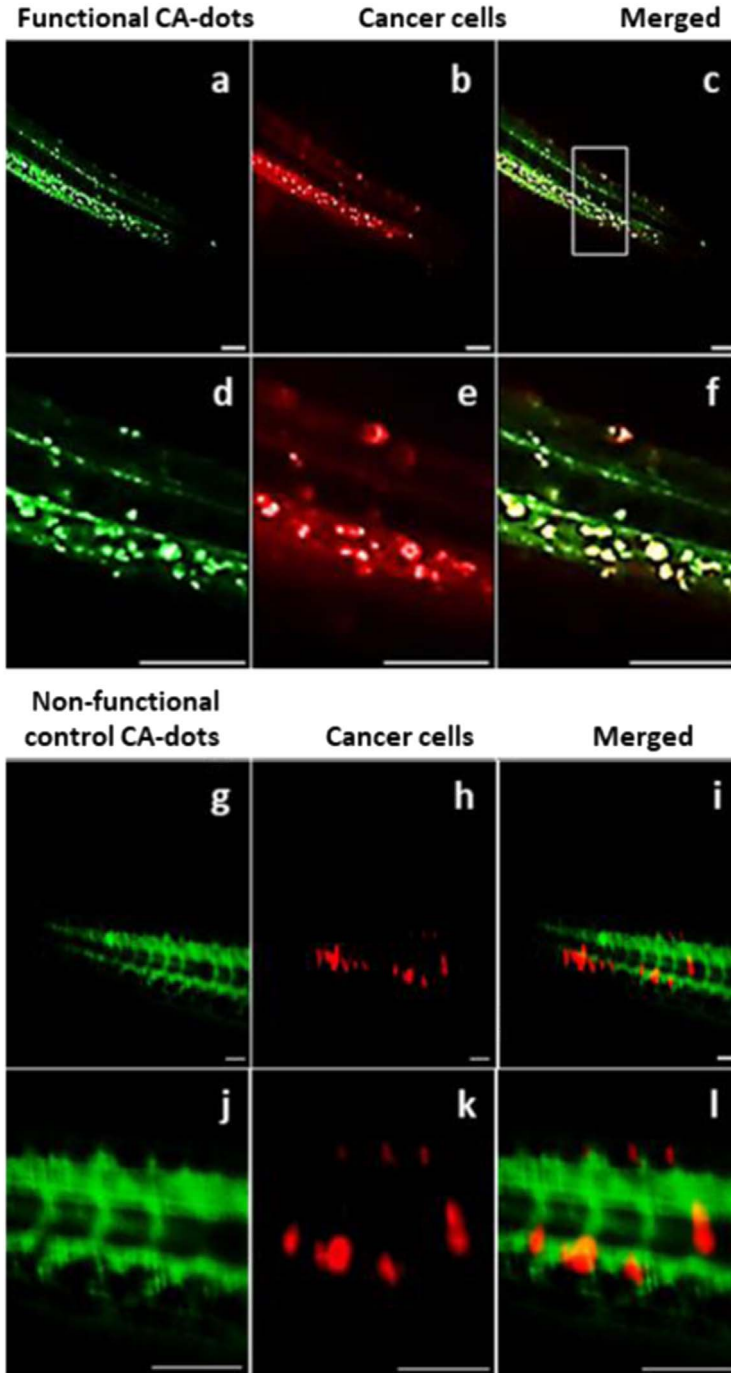
Fig. 6. Localization of CA-SB-PEG-FA (a,d) nanoparticles and cancer cells (b,e) in zebrafish 30 min following injection. Particle-cancer cell colocalization (c,f) can be seen as yellow color after merging of green and red channels. The top panel shows the full zebrafish tail. The bottom panel is a zoomed section demonstrating clear evidence of cancer targeting. Localization of CA-SB-PEG (a,d) nanoparticles and cancer cells (b,e) in zebrafish 30 min following injection. Ideally, particle-cancer cell colocalization (c,f) can be seen as yellow color after merging of green and red channels. The top panel (a-c) shows the full zebrafish tail while the bottom panel (d-f) is a zoomed section demonstrating little evidence of cancer targeting. Scale bar is 100 μm.
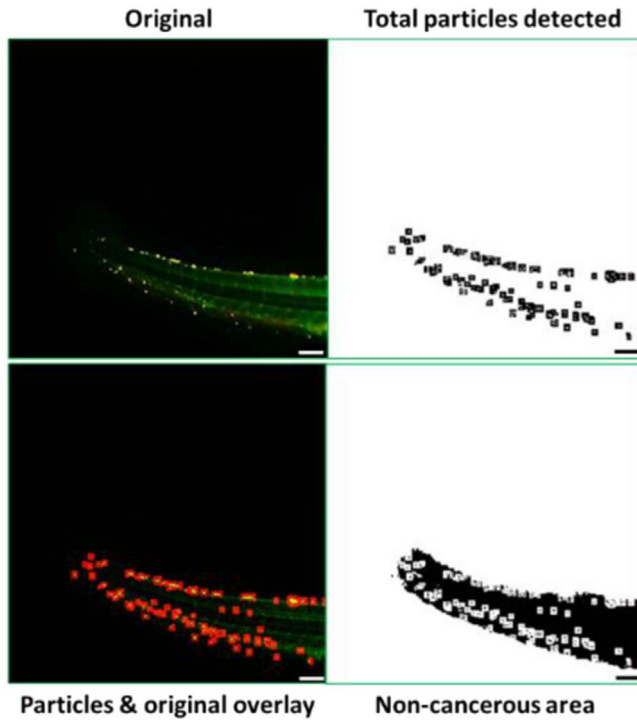
Fig. 7. Sensitivity-Specificity analysis was performed on the 50 min merged fluorescence image of folate-functionalized nanoparticles. Scale bar is 100 μm.
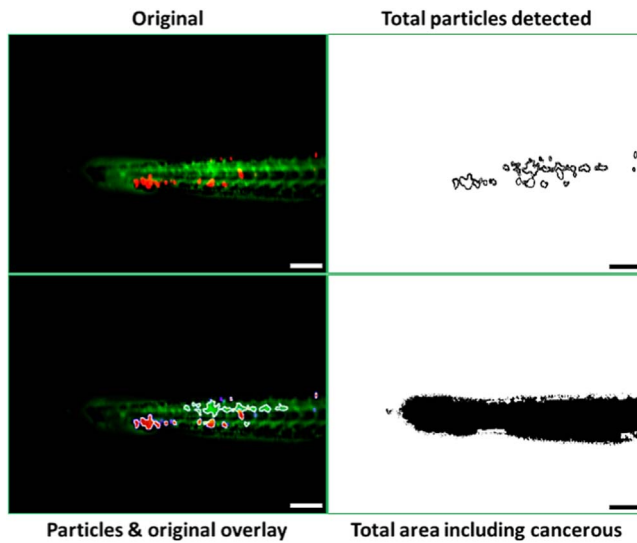
Fig. 8. Sensitivity-Specificity analysis was performed on the 50 min merged fluorescence image of control PEGylated nano-particles. Scale bar is 100 μm.

To calculate the efficiency of PF127-folic acid synthesis, the number of folic acid per PF127 molecule was estimated. Absorbance (Fig. 3) and known extinction coefficient [6–9] was used to calculate the concentration of folic acid (in moles/liter). Concentration of PF127 in moles/liter was calculated using concentration in mg/mL and molecular weight. Number of folic acid per PF127 molecule is the ratio of concentration of FA is to concentration of PF127. A maximum of 2 folic acid groups can be attached per PF127 molecule, so the efficiency of folic acid attachment is ~60%, or 1.22 folate molecules per polymer chain at 282 nm.

Given that a CA-dot particle is comprised of roughly 25% guest polymer, there are approximately 1.71E-8 mol of guest polymer per mL of nanoparticles and thus, 1.03E16 polymer chains. If 1.22 folate molecules are attached per polymer chain, there are ~1.26E16 folate groups present per mL of nanoparticles. Provided the density of cellulose acetate (1.29 g/ml), the known nanoparticle concentration (1 mg/ml) as well as the measured particle diameters (obtained via DLS or AFM), we can calculate the total number of 50 nm diameter nanoparticles and subsequently, the amount of folate groups per single nanoparticle. We calculate that each targeted nanoparticle possesses 1450 ± 330 folate molecules.

The number of folic acid groups per nanoparticle was also calculated using the absorbance and extinction coefficient at 282 nm. To remove the contribution from non-folic acid components, the absorbance of each fluorescent particle was first normalized to that of the folate-conjugated nanoparticles using the encapsulated dye peak (Fig. 4). Differences in absorbance at 282 nm between conjugated and unconjugated particles were attributed to folic acid contribution. Each 0.01 mg/ml concentration of folic acid contributes 0.56 absorbance units, so the amount of folate groups per type of biofunctionalized nanoparticle ranged around 1000 molecules/particle (870 ± 220 folates/Stilbene particle, 910 ± 200 folates/Rhodamine 560 particle, 1110 ± 180 folates/Tracer Yellow particle, and 930 ± 290 folates/Methylene Blue particle). Like the Raman analysis of folate/particle calculation, not all folate groups are necessarily exhibited on the surface. When comparing the two approaches, there appears to be reasonable agreement in folate estimation.

2.4. Methods for image analysis of particle-cancer cell colocalization: calculation of sensitivity, specificity, and accuracy

Nanoparticle (green) and tumor (red) fluorescence images were merged to form a composite image illustrating colocalized and non-colocalized regions. Color threshold was adjusted to brightness level 155 as a pre-processing step. ImageJ Particle Size package was utilized to detect regions of tumor and particle fluorescence by assigning a size threshold value (0.1 to Infinity) to the particle detection algorithm.

To quantify ability of CA-dots to target tumors in the zebrafish model, we calculated sensitivity, specificity, and accuracy of this targeting method. Since cancer and particle fluorescence spectra are distinctly separate and observed in different channels, both particles and tumors can be directly identified, and their colocalization in space verified (Figs. 5 and 6). We used ImageJ software with the particle analysis plug-in to classify colocalization of cancer vs. particle fluorescence into the four core confusion matrix categories: True positive (TP, correct identification of tumor), True negative (TN, correct identification of healthy tissue), False positive (FP, incorrect identification of tumor), and False negative (FN, incorrect identification of healthy tissue).

In Fig. 7, the top left panel labeled "Original" is the acquired microscope image. In the top right panel labeled "Total particles detected," ImageJ finds all instances of fluorescent regions whether it be from untargeted tumors, targeted tumors, or nonspecifically accumulated nanoparticles utilizing the pre-processing and thresholding steps aforementioned. The bottom left panel, "Particles and original overlay" illustrates good co-registration between the original image and the ImageJ processed image. Now, utilizing images shown in Fig. 2a-f of Ref. [1], and processing step-wise as shown in Fig. 7, one can classify each fluorescent image (as exhibited in the "Total particles detected" panel) into confusion matrix categories. We found 58 instances of TP, FP, and FN classifications and 264 instances of TN in the folate-functionalized targeting nanoparticles (evaluated by assessing non-cancerous and non-targeted areas and dividing into representative particle areas; the threshold to separate cancer from noncancer was chosen to be 0.1). Sensitivity, specificity, and accuracy were calculated using standard

definitions:

$$Sensitivity \quad = \quad TP/(TP+FN) \tag{2}$$

$$Specificity \quad = \quad TN/(TN+FP) \tag{3}$$

$$Accuracy \quad = \quad (TP+TN)/(TP+TN+FP+FN) \tag{4}$$

Using the numbers obtained above, one can find a sensitivity of 96%, a specificity of 96%, and an accuracy of 96%. For the control particles (shown in Fig. 2g–l of Ref. [1]), similar data processing results in 29 instances of TP, FP, and FN classifications and 49 instances of TN (processing step-wise as shown in Fig. 8). This gives a sensitivity of 65%, a specificity of 80%, and an accuracy of 76%. This is clearly less than the values obtained with the targeting particles.

Acknowledgments

Transparency document. Supporting information

Transparency data associated with this article can be found in the online version at https://doi.org/10.1016/j.dib.2018.12.030.

References

[1] B. Peng, et al., Ultrabright fluorescent cellulose acetate nanoparticles for imaging tumors through systemic and topical applications, *Materials Today* (2018), in press, https://doi.org/10.1016/j.mattod.2018.11.001.
[2] V. Kalaparthi, et al., The nature of ultrabrightness of nanoporous fluorescent particles with physically encapsulated fluorescent dyes, J. Mater. Chem. C 4 (2016) 2197–2210. https://doi.org/10.1039/c5tc04221f.
[3] S. Palantavida, et al., Ultrabright nir fluorescent mesoporous silica nanoparticles, J. Mater. Chem. B 2 (2014) 3107–3114. https://doi.org/10.1039/c4tb00287c.
[4] E.B. Cho, et al., Ultrabright fluorescent mesoporous silica nanoparticles, Small 6 (2010) 2314–2319. https://doi.org/10.1002/smll.201001337.
[5] S. Palantavida, et al., Ultrabright fluorescent silica particles with a large number of complex spectra excited with a single wavelength for multiplex applications, Nanoscale 9 (2017) 4881–4890. https://doi.org/10.1039/c6nr08976c.
[6] J. Chen, et al., Substrate-triggered exosite binding: synergistic dendrimer/folic acid action for achieving specific, tight-binding to folate binding protein, Biomacromolecules 17 (2016) 922–927.
[7] B.D. Smith, et al., Site-specific folate conjugation to a cytotoxic protein, Bioorg. Med. Chem. Lett. 21 (2011) 5029–5032.
[8] I.V. Dimitrov, et al., A mild and versatile approach for DNA encapsulation, Soft Matter 7 (2011) 8002–8004.
[9] G.F. Ball, Vitamins in Foods: Analysis, Bioavailability, and Stability, CRC Press, 2005.